Materials and Structures (2018) 51:159
https://doi.org/10.1617/s11527-018-1285-x

Cavitation of water in hardened cement paste under short-term desorption measurements

Ippei Maruyama · Jiří Rymeš · Matthieu Vandamme · Benoit Coasne

Received: 4 October 2018 / Accepted: 19 November 2018 / Published online: 26 November 2018

Abstract Water vapor sorption isotherm measurement is one of the promising techniques to understand the microstructure of hardened cement paste, because it always gives a higher surface area than sorption isotherm measurements performed with other adsorbents such as nitrogen and argon, which implies that water molecules can probe the widest range of the microstructure of hardened cement pastes. When, at 20 °C, the water sorption measurement is conducted such as to last for a few days, a characteristic behavior—a sudden drop in adsorbed amount around a relative humidity of 0.35—is always observed on the desorption branch. Here, we prove that this sudden drop is caused by water cavitation, based on an analysis of experimental sorption isotherms acquired at various temperatures, scanning isotherms, and length-change isotherms. Cavitation in hardened cement paste is likely to occur in the C–S–H gel pores constricted by the C–S–H interlayer space.

I. Maruyama (✉) · J. Rymeš
Graduate School of Environmental Studies, Nagoya University, Nagoya, Japan
e-mail: ippei@dali.nuac.nagoya-u.ac.jp

M. Vandamme
Laboratoire Navier, UMR 8205, École des Ponts ParisTech, IFSTTAR, CNRS, Champs-sur-Marne, France

B. Coasne
Univ. Grenoble Alpes, CNRS, LIPhy, 38000 Grenoble, France

Keywords Water vapor sorption isotherm · Cavitation

1 Introduction

Understanding of the microstructure of hardened cement pastes (hcp) is a key issue for a variety of applications of cement-based materials. Because one of the Portland cement hydrates, namely calcium silicate hydrates (C–S–H), exhibits a colloidal nature [1], gaining such an understanding is difficult. Many reactions in Portland cement systems and physical properties of cement-based materials are associated with water, so that techniques using water as a probe to detect features of the microstructure are of significant interest. Water vapor sorption isotherms are strongly impacted by the microstructure and surface chemistry of the tested material: consequently, water sorption isotherms are one of the promising techniques to understand the microstructure of hcp.

When a water vapor sorption isotherm is measured on a hcp, generally, a sudden drop of the adsorbed amount is observed on the desorption, around a relative humidity (which is the term used to designate relative pressure in the case of water, and will be noted RH) of 0.40 [2]. Generally, the hysteresis of the water vapor sorption isotherm measured on hcp has been explained by the ink-bottle effect (which explains that

different pores can be filled on the adsorption and on the desorption branch) and/or by the kinetics of moisture transport [3, 4].

During adsorption or desorption, the surface tension acting on the meniscus causes negative pressure in the condensed liquid water. This negative pressure stretches the liquid water entrapped in the pores connected to the ambient atmosphere through necking pores. When water vapor is more stable than liquid water (which is the fact for any relative humidity lower than 100%), the nucleation of a bubble of the vapor phase in the thus metastable liquid phase—a phenomenon known as cavitation—can occur. To observe such a nucleation of bubble from the metastable liquid phase, an energy barrier must be overcome. However, when the negative pressure becomes too large (in absolute value), the liquid water becomes unstable, the nucleation of vapor bubbles must occur and suddenly a certain amount of water is released from the sample: the pressure at which the liquid state becomes unstable is called the cavitation pressure.

Recently, the occurrence of cavitation on the desorption branch of sorption measurements has been discussed in the field of sorption science [5–9], as a sudden drop in adsorbed amounts was observed upon desorption for a variety of adsorbates and mesoporous materials. Researchers observed that, for a given adsorbate and at a given temperature, when a sudden drop occurs on the desorption branch, this drop occurs roughly always at the same relative pressure, independent of the adsorbent. They also observed that, when scanning isotherms are performed, if a sudden drop occurs on the various desorption branches, again this sudden drop occurs roughly always at the same relative pressure. From those observations, one can infer that the sudden drop happens regardless of the size of the adsorbate-filled pores. Consequently, researchers concluded that the sudden drop does not pertain to the so-called pore blocking effect (i.e. when an ink-bottle pore empties as the constriction desorbs) but to cavitation (i.e. an instability in the pore system containing ink-bottle pores whose diameter of the neck is less than a threshold value). This conclusion has also been proved with numerical calculations [6, 10].

In this contribution, aiming at exploring the hypothesis that the sudden drop observed on the desorption branch of the water vapor isotherm measured on hcp corresponds to cavitation, systematic experiments were conducted and discussed, to prove or disprove this hypothesis.

2 Experiments

2.1 Materials

Cement samples were prepared using a Japanese white Portland cement with water-to-cement mass ratio w/c of 0.55. The chemical composition of the cement is given in Table 1.

All the materials for sample preparation were stored in a thermostatic room (20 ± 1 °C) for a few days prior to mixing. The cement was mixed with tap water in a Hobart mixer for 3 min and then the fresh paste was repeatedly remixed every 30 min for about 5–6 h to prevent bleeding during the dormant period. After that, the mixture was poured into 3 × 13 × 300 mm molds and compacted on a vibration table. The hcp samples were sealed-cured in the thermostatic room, demolded at the age of 4 days and then further cured in lime-saturated water. At the age of 180 days, the hcp samples were placed into an 11% RH chamber (notation: W55-11) and equilibrated there for more than 6 years. A saturated LiCl solution was used to control the RH. The hcp samples were kept in the lime-saturated water (notation: W55-SAT) until the day of measurement (about 6.5 years). The details can be found in previous reports [11, 12].

Hcp samples containing a shrinkage reducing agent (SRA) (notation of the samples: W55SR-11), were prepared by following the same procedure as for the hcp samples containing no SRA, but for the facts that part of the water (corresponding to 3% of the mass of clinker) was replaced with the SRA, and that the samples were cured in a lime-saturated water at a concentration of SRA in water equal to 5.45%. After 180 days of curing, the W55SR-11 samples were stored at 11% RH and 20 ± 1 °C, until equilibrium was reached. Details are provided in the following Ref. [13].

Hierarchical zeolites were synthetized in the same manner as in a previously published study dealing with the cavitation phenomenon [6]. ZSM-5, a high-silica (SiO_2/Al_2O_3 = 40) zeolite, was purchased from Tosoh Corporation and used as a starting material. Z40-H was prepared by alkali treatment in aqueous NaOH (0.2 M) at the boiling temperature of the solution for

Table 1 X-ray fluorescence elemental analysis of the white Portland cement used for the HCP samples

Ig. loss	SiO_2	Al_2O_3	Fe_2O_3	CaO	MgO	SO_3	Na_2O	K_2O	TiO_2	P_2O_5	MnO	Cl	Sum
2.93	22.43	4.67	0.16	65.69	0.98	2.51	0.00	0.07	0.17	0.03	0.00	0.00	99.64

30 min, and then oven-dried at 105 °C. Z40-HW was prepared from Z40-H by washing the remaining NaOH away from the porous system, by stirring the powder in a large amount of distilled water for 20 h. Reagent calcium hydroxide (referred as portlandite) and Mobil Crystalline Material 41 (MCM-41, 643645, Aldrich, silica-type with pores with a size of 2.5–2.7 nm) were used in the part of the study dedicated to the measurement of sorption isotherms at various temperatures. A monolithic sample made from MCM-41 was prepared by compaction (i.e., by pressing MCM-41 particles together) following the Ref. [14] for the part of the study dedicated to length-change isotherm measurements.

2.2 Methods

Sorption isotherms at various temperatures were obtained with the manometric (volumetric) method with a sorption analyser (VSTAR, Quantachrome Instruments) at temperatures of 20, 40, 60, and 80 °C. A sample of about 25 ± 1 mg was used for each measurement. Since some cement hydrates are considered to be unstable at elevated temperatures [15], the vacuum-drying of the hcp samples was performed at room temperature. The hcp samples were vacuum-dried again at 105 °C at the end of each measurement and the sorption amount was normalized with respect to this mass. A freshly crushed hcp powder (with grains with a size of about 25–75 μm) was used for each measurement. The hierarchical zeolite samples were vacuum-dried (with an ultimate vacuum pressure of the pump equal to 0.7 Pa) at room temperature until dry, and the portlandite powder was vacuum-dried at 105 °C for 1 h. MCM-41 was vacuum-dried at 200 °C for 1 h. For all samples, during their vacuum-drying, the pressure increase around the sample in a closed system of the vacuum-drying apparatus was regularly monitored, and we considered that the dry state was reached when the partial pressure remained stable and equal to about 3 Pa, which was typically achieved within 45–60 min of vacuum-drying for the hcp samples.

Scanning sorption isotherms were measured on samples W55-SAT and W55-11. The maximum relative humidity was set from 0.95 to 0.50. But for this feature, the protocol for measuring the scanning sorption isotherms was the same as for measuring the sorption isotherms at various temperatures, and results were normalized with respect to the dry mass of the sample at 105 °C.

Length-change isotherms for samples W55-11, W55SR-11 and MCM-41 were obtained with a thermomechanical analyzer (TMA) coupled with an RH generator (TMA4000SA and HC9700, Bruker AXS). Length changes were measured with a linear variable differential transformer (LVDT) with a precision of 0.5 μm, a minimum resolution of 0.0025 μm, and a contact load of 0.098 N. The W55-11 and W55SR-11 samples were incrementally dried from 0.11 RH to 0.05 RH, after which they were incrementally re-humidified up to 0.90 RH. Finally, they were incrementally re-dried back to 0.11 RH. In case of the monolithic sample MCM-41 obtained by compaction, the RH was first set as 0.70 RH and then decreased incrementally down to 0.05 RH, after which it was increased back up to 0.90 RH, and then decreased back to 0.70 RH. All length-change isotherms were measured at 20 ± 0.1 °C. For each step, the RH of the atmospheric flow was kept constant for 5 h for W55-11 and W55SR-11 and 8 h for the monolithic MCM-41 sample obtained by compaction. For some steps, the length change did not have time to reach an equilibrium value, but the impact of capillary condensation on the shrinkage strain was evident; therefore, this process was considered to be acceptable with regard to the objectives of this research. On the same samples, sorption isotherm data were collected using a thermogravimetry analyzer coupled to an RH generator (TG–DTA 2000SA and HC9700, Bruker AXS). After the same RH steps as those used for the measurement of the length-change isotherms, the samples were heated at 105 °C under nitrogen gas

flow until reaching equilibrium, which provided the reference condition with respect to which adsorbed amounts were normalized.

3 Results and discussion

3.1 Dependence on temperature

Temperature-dependent water vapor sorption isotherms are shown in Fig. 1. For all samples but W55-11 (see Fig. 1b), the adsorption branches did not depend significantly on temperature. In case of sample W55-11, the sorption amount on the adsorption branch increased as the measurement temperature increased. Due to the increased mobility of water molecules with temperature, calcium silicate hydrate (C–S–H), whose microstructure evolves in the long term when subjected to variations of relative humidity, was more re-humidified during adsorption and hence subjected to more significant re-organizations of its microstructure when temperature was increased, which could have increased the sorption amount. In case of sample W55-SAT, the alteration of C–S–H at higher temperature (which might have happened during drying performed as a pre-treatment before measurement) might contribute to the decrease in sorption in the range of relative humidities below 0.7 [16–18]. The re-organization of C–S–H related microstructure has been confirmed by 1H-NMR relaxometry measurement [19, 20]. Elevated temperature causes moisture redistribution in the sealed hcp, a release of water from interlayer spaces and the released water go into gel pores [20]. Consequently, in the open condition, the lower sorption is realized in the higher temperature condition at a given constant relative humidity. This behavior is well consistent to the what we observed in the case of W55-SAT.

For all samples, desorption branches depended remarkably on temperature. In case of sample W55-SAT, the maximum adsorption commonly attained about 230 mg/g-dried hcp. The gradient of desorption isotherm in the highest RH range (i.e., above the sudden drop in adsorbed amount) depended on temperature and was steeper when the measurement temperature was higher. The positions of starting of sudden drop (PSSD) on the desorption branch (i.e., the relative humidities at which, on the desorption branch, the sudden drop started) were 0.36, 0.44, 0.50, 0.54 at 20, 40, 60, and 80 °C, respectively. After the sudden drop, the desorption branches at different temperatures remained different from each other, down to a relative humidity of $\sim$ 0.03.

In case of sample W55-11, above the PSSD and in the low RH range (i.e., at relatives humidities below 0.4) the desorption trend was similar at 60 and at 80 °C. The maximum adsorbed amounts at 40, 60, and 80 °C were comparable, while that at 20 °C was smaller than at the other 3 temperatures. Moreover, the features of the desorption branch (typically, the PSSD and the sorption amounts) at 40 °C were almost between those at 20 and 60 °C. The sorption amount at 40 °C was very close to that measured at 60 °C in the higher RH range, but gradually came closer to that measured at 20 °C when the relative humidity approached the PSSD. Below a relative humidity of 0.35, the sorption isotherm at 40 °C was almost the same as that measured at 20 °C. Such similarity can be explained by the microstructural re-organization during heating/cooling and/or drying/rehumidifying. The PSSD on the desorption branch were 0.35, 0.43, 0.48, and 0.52 at 20, 40, 60, and 80 °C, respectively. Such values are in good agreement with those measured for sample W55-SAT.

The dependence of the desorption slopes on temperatures for sample W55-11 contrasts with what is observed for sample Z40-HW. For this latter sample, except for the PSSD, the features of the desorption branch were independent of temperature. The PSSD were very close to those measured for samples W55-SAT and W55-11. Regarding the case of the Portlandite powder, other than the PSSD, the overall features of the desorption branch were very similar to those of sample Z40-HW. The PSSD for sample Z40-H, in which many alkali metal ions remained in the system, differed from the PSSD for other samples. Generally, the PSSD for sample Z40-H were smaller by about 0.07 (in terms of relative humidity) than those for sample Z40-HW, while the other features of the desorption branch for this former sample remained quite similar to those of sample Z40-HW. The anomaly of this former sample will be discussed later.

Based on previous studies in sorption science [6], this sudden drop has been explained by either ink-bottle effect or cavitation. If the sudden drop is related to the ink-bottle effect, the relative pressure at which this sudden drop occurs (i.e., the PSSD) should depend on the pore structure, as it is related to the size of the

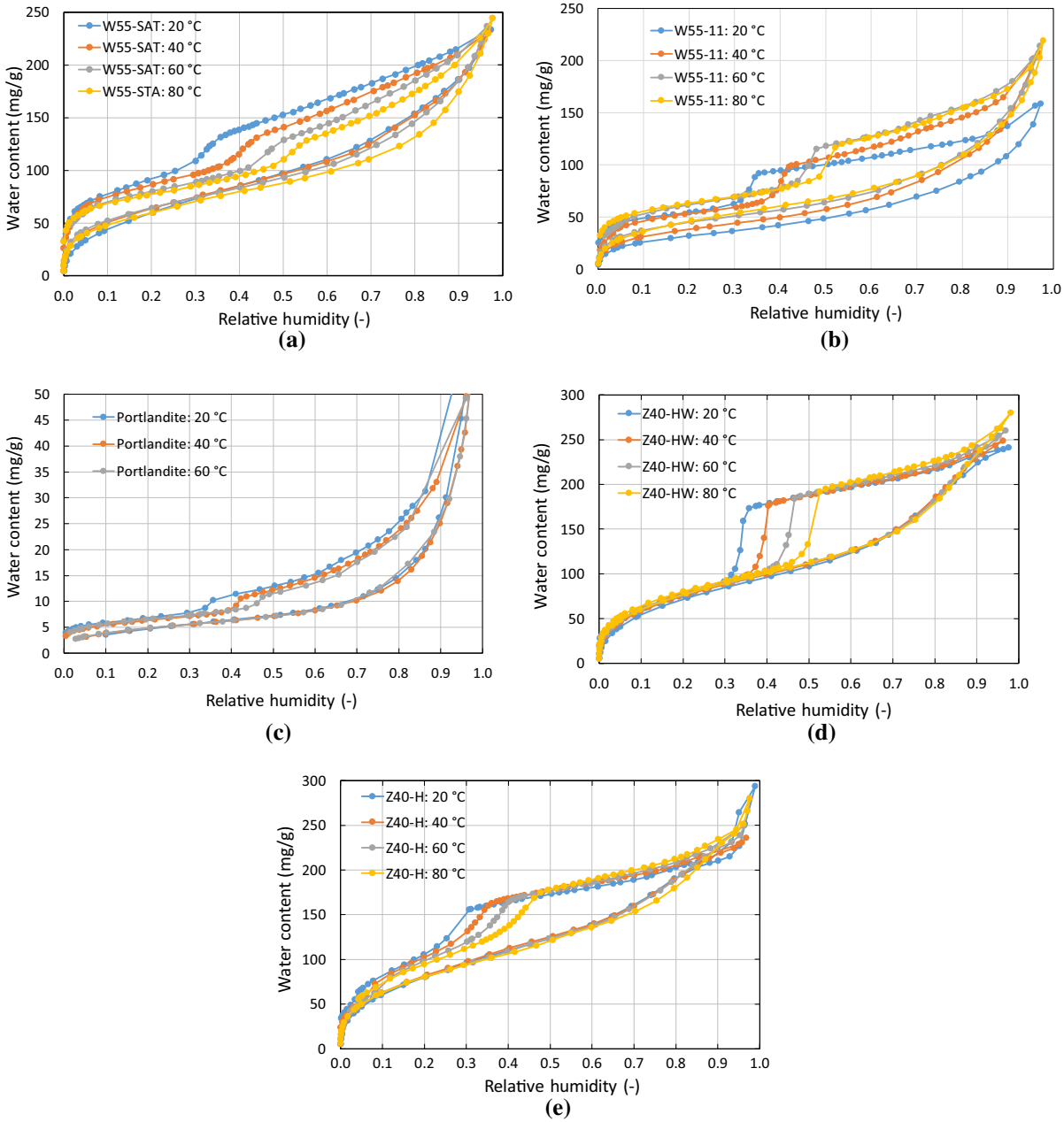

Fig. 1 Sorption isotherms measured at various temperatures, showing that the relative humidity at which a sudden drop of adsorbed amount is observed on the desorption branch depends on temperature: **a** Saturated hardened cement paste (W55-SAT), **b** hardened cement paste previously dried at 11% RH (W55-11), **c** portlandite powder, **d** washed hierarchical alkali-treated zeolite (Z40-HW), and **e** hierarchical alkali-treated zeolite (Z40-H)

necks (i.e., constrictions) between larger pores. In contrast, if the sudden drop is due to cavitation, the relative pressure at which this sudden drop occurs should not depend on the pore structure, as it is mostly a characteristic of the fluid (i.e., of its nature and of its chemical composition).

By comparing the data, especially for samples W55-SAT, W55-11, Z40-HW, and Portlandite, there is clearly no doubt that the water cavitation occurs at a

relative humidity of about $\sim$ 0.35 at room temperature (as evidenced by the sharp drop in desorption branch). First, we thus observe that the PSSD is clearly sample-independent. For a general sample with a broad pore size distribution, there is no reason why the size of all necks should be identical from sample to sample: this is especially the case for the Portlandite powder, whose microstructure is expected to differ significantly from that of the other samples tested in this study. Consequently, the fact that the sudden drop in adsorbed amount occurs at the same relative humidity on different samples hints toward a sudden drop that is due to cavitation. Second, indeed, cavitation for bulk water occurs at a relative humidity of about $\sim$ 0.35 [21]. For water in zeolite, the same kink/sharp desorption at this relative humidity was observed.

Cavitation pressures p_c were calculated for each sample and temperature using Kelvin equation $p_c = (RT/v_l)\ln(RH/(1-x))$, where R = 8.314 J/mol/K is the ideal gas constant, T is the absolute temperature, v_l is the molar volume of the pore liquid (considered to be equal to 1.8e−5 m^3/mol and temperature independent), RH is the relative humidity at which the sudden drop on the desorption branch is observed (i.e., the PSSD), and x is the mole fraction of dissolved salts (taken equal to 4e−4 for $Ca(OH)_2$ and to 0.03 for hcp as estimated by the RH measurement data for hcp collected by Aili et al. [22]). The calculated cavitation pressures are summarized in Fig. 2a. For comparison, this figure also displays estimated cavitation pressures obtained with the following models: (1) basic theory with thin wall approximation (TWA), (2) Density functional theory (DFT) with a Van der Waals equation of state (EOS) proposed by Speedy [23], and (3) DFT with EOS calculated by molecular dynamics simulations using the five-site transferable interaction potential (TIP5P) [24]. All the estimated cavitation pressures are taken from references [25–27]. The magnitude of the measured cavitation pressure is very close to that estimated with the models. Especially, the cavitation pressures for samples W55-SAT, Portlandite, and Z40-HW show good agreement with the estimation calculated with DFT with the Speedy EOS. Moreover, the magnitude of the variations of cavitation pressure due to variations of temperatures, as calculated with the DFT-TIP5P and TWA models, is consistent with the measured magnitude of those same variations. This additional information also supports the hypothesis that the sudden drop in the desorption branch is caused by cavitation.

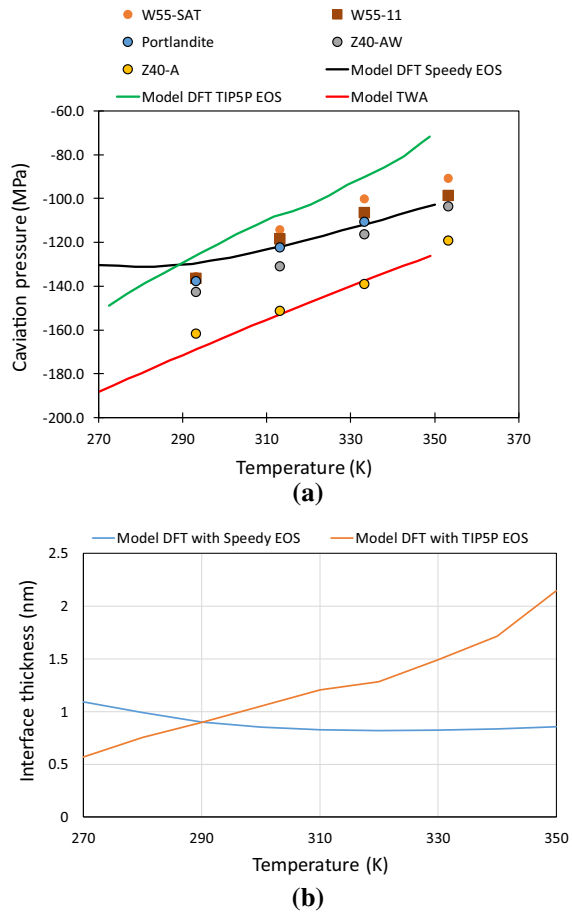

Fig. 2 **a** Cavitation pressure measured on the various samples and predicted by modeling. Lines are cited from Herbert et al. [25]. Here, the experimental cavitation pressure is calculated by using the relative humidity at the beginning of sudden drop in desorption branch and Kelvin equation. **b** Liquid–vapor interface thickness calculated with DFT models. Data are cited from Caupin [23]

For cavitation to occur, vapor nuclei need to be able to form in confined pores, which requires the pores to be of sufficient thickness, because the vapor nuclei need to form an interface between liquid and vapor. Based on the DFT Speedy EOS calculation, the thickness of this interface is estimated to about $\sim$ 0.8 nm, and, therefore, the diameter of pores in which cavitation can occur should be greater than 1.6 nm. On top of that, if we add the thickness of the liquid film adsorbed on solid surfaces [28], we find out that cavitation can only occur in pores larger than 2.3 nm.

These minimum sizes for the confined pores in which cavitation can occur are consistent with the size of the C–S–H "gel pores" [29–32].

Recently, ^{1}H-NMR relaxometry has been applied to cement paste [33–40]. Based on the data of a Carr–Purcell–Meiboom–Gill (CPMG) pulse sequence experiment and application of an inverse Laplace transform algorithm, four different T_2 peaks of mobile water in hcp were identified. These T_2 values are considered to be related to the mobility of interlayer water, gel-pore water, interhydrate-pore water, and capillary pore water [38]. Integration of the peak intensity represents the corresponding mass of mobile water. The interlayer spaces in-between C–S–H layers are considered to be the smallest pores containing mobile water. When T_2-T_2 correlation is measured, it is possible to obtain information about pore connectivity, within the limit of a characteristic time of the mobility of water molecules, which is represented by a waiting time, which is one of the measuring parameters. McDonald et al. [41] showed that the water is easily exchanged between interlayer spaces and gel pores, and little exchanged between capillary pores and interlayer spaces, or between capillary pores and gel pores. These trends are also confirmed by recent experimental observation [20]. Based on the experimental facts about water mobility, pore distribution, pore connectivity in hcp, and on the cavitation data here presented, the most probable spaces in which cavitation occurs are the C–S–H gel pores or the capillary pores, in which liquid water would still be present at the relative humidity corresponding to the PSSD, because those pores would be connected to the surrounding through narrow interlayer spaces.

This tentative interpretation can also be supported otherwise. Indeed, Fig. 2a shows that, for the cement pastes W55 and W55-11, the cavitation pressures are around $-$ 140 MPa at 20 °C and $-$ 100 MPa at 80 °C. Using Laplace equation $\Delta p = 2\sigma/R$, where σ is the surface tension of water (considered to be equal to 72.74 mJ/m^2 at 20 °C, and 62.64 mJ/m^2 at 80 °C, by linear interpolation of references values [42]), we find corresponding radii of the liquid–vapor menisci of 1–1.25 nm. Consequently, when cavitation is observed, cavitation must have occurred in pores with a radius larger than about 1 nm, and connected to their surroundings through necks with radius smaller than about 1 nm. Such numbers are consistent with the interpretation of cavitation occurring in spaces connected to their surroundings through C-S–H interlayer spaces.

For samples W55-SAT and W55-11, the loss of water associated to the sharp drop is always around 30 mg/g and is independent of temperature (see Fig. 1a, b). Consequently, when cavitation occurs, for 1 g of sample which, for a density of 1.55 g/cm^3, represents a sample of about 645 mm^3, a volume of water of 30 mm^3 should cavitate, i.e., a volume of about 5% of the volume of the sample. According to Power's hydration model [43], the volume of gel porosity after full hydration of the clinker is equal to $0.6(1 - p)$, where p is the volume fraction of water in the initial mix of the cement paste, and is equal to $p = (w/c)/((w/c) + (\rho_w/\rho_c))$, where $\rho_w = 1$ g/cm^3 is the mass density of water and $\rho_c = 3.15$ g/cm^3 is the mass density of clinker. For a typical paste with $w/c = 0.55$, we find that $p = 0.64$ and that the gel porosity occupies about 21% of the volume of a typical paste, which needs to be compared to a volume of cavitating water equal to about 5% of the volume of the same paste. Consequently, the idea that the liquid water that cavitates is mostly contained in the C–S–H gel porosity seems reasonable.

The measured cavitation pressures slightly differed from sample to sample, especially for sample Z40-H. We can propose several explanations for these differences. One explanation can be the effect of dissolved ions, which could explain the difference in cavitation pressures measured in cement paste, zeolite, and portlandite, for which the chemistry of the pore solution must be specific to each sample. In the case of the unwashed zeolite Z40-H, some precipitated sodium hydroxide exists on the surface zeolite and can easily dissolve upon humidifying during the measurement. A second explanation can be the effect of hydrophobicity of the pore surface, which may explain the difference in measured cavitation pressures in the washed (Z40-HW) and the unwashed (Z40-H) zeolites. Cavitation was reported to be more likely when the pore surfaces are hydrophobic than hydrophilic [44]. Precipitated sodium hydroxide, which provides some hydrophilicity to the surface of pores, should decrease the cavitation pressure. On the contrary, when a shrinkage reducing agent (SRA) is used, which is composed of alcohol-ethylene oxide polymers with a better hydrophilic-lipophilic balance, we observe that the cavitation pressure is increased (see Fig. 3). Indeed, when the Z40-HW sample or the W55 sample

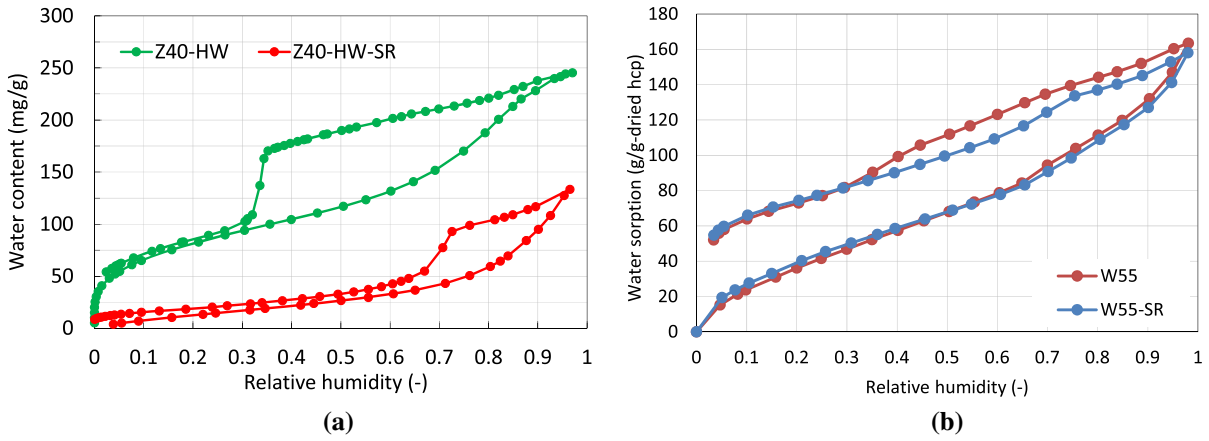

Fig. 3 Modification of the adsorption isotherm by addition of a shrinkage reducing agent (SRA) in zeolite sample (**a**) and Hcp sample (**b**) (data is cited from Maruyama et al. [48]). The addition of SRA shifts the PSSD to larger relative humidities, i.e., up to about 0.7

contains SRA, the PSSD is shifted to larger relative humidities, around $\sim$ 0.7. In this case, the lipophilic part of the SRA molecule modifies the apparent property of the pore surface, making it hydrophobic, which increases the cavitation pressure. Such a hydrophobic/hydrophilic surface effect can be understood as follows. While cavitation is expected as a first order approximation to be a surface-independent effect inherent to the fluid, it cannot be ruled out that in nanopores the interaction with the host surface affects the cavitation pressure. Indeed, upon nucleating a gas bubble inside tiny pores, the coupling between the solid/liquid and liquid/gas interfaces induces important disjoining pressure effects. Such additional interaction terms in confinement can modify the pressure at which cavitation occurs for the bulk liquid taken at the same temperature. Moreover, hydrophobic surfaces should promote cavitation (therefore occurring at larger pressure i.e. lower suction) as the liquid density is necessarily smaller at the interface than with hydrophilic surfaces. Such lower densities in the surface vicinity are expected to facilitate the occurrence of small gas bubbles.

3.2 Scanning sorption isotherm

Scanning sorption isotherm experiments were conducted on samples W55-SAT and W55-11. The results are summarized in Fig. 4. For a given starting point upon the adsorption branch, all pores with a size smaller than a threshold value that depends on relative humidity are filled with liquid water. In Fig. 4, cavitation is observed on the desorption branch of the sorption isotherms with a returning point greater than 0.65. From this observation, we infer that pores with different sizes (since various returning points were probed) exhibit a sudden loss of water, all at the same relative humidity around $\sim$ 0.35. Such result is an additional evidence of the cavitation, which must occur in pores of any size at once.

In addition, cavitation was not observed on the sorption isotherm with a returning point at 0.50, while cavitation was observed on the sorption isotherm with a returning point at 0.65. Therefore, the upper bound of the radius of the smallest pores in which cavitation can occur is 2.5 nm (if the statistical thickness of the liquid layer adsorbed on solid surfaces is excluded) or 3.2 nm (if the statistical thickness of the liquid layer adsorbed on solid surfaces, as given by [28], is included). The corresponding diameters are 5.0 and 6.4 nm, respectively.

Based on the discussion in references [9, 45], for a given temperature T, no phase transition (i.e., capillary condensation, cavitation, etc.) can occur in a pore of diameter D that verifies $D < D_c$, where D_c is a critical diameter given by $D_c = 4\sigma T_c/(T_c - T)$, with T_c the critical temperature of bulk water and σ = 0.28 nm the size of the water molecule. For T = 293.15 K, we find D_c = 2.05 nm, which suggests that the C–S–H interlayer spaces that constrict liquid water in gel or capillary pores are smaller than 2.05 nm. This calculation also means that cavitation should be observed in pores whose diameter is greater than 2.05 nm. In accordance with this value, it has been reported that, in

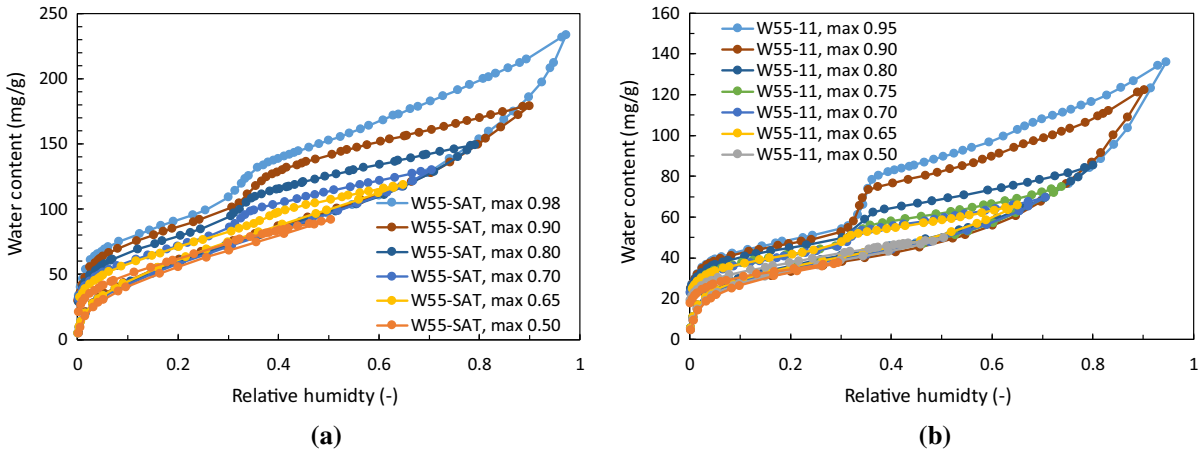

Fig. 4 Scanning sorption isotherms on samples W55-SAT (**a**) and W55-11 (**b**), acquired at 20 °C

a hierarchical zeolite and in MCM-41, cavitation of water occurs in pores with a diameter of ~ 2.5 nm [10, 21]. However, this critical diameter is not consistent with our discussion of Fig. 4, since we observed no cavitation of water in pores with a diameter smaller than 5.0 nm (or 6.4 nm if the statistical thickness of the liquid layer adsorbed on solid surfaces is included). Therefore, the minimum diameter of the pores in which cavitation is possible could be signficantly smaller than values of 5.0 nm (or 6.4 nm) estimated earlier.

Several explanations for this discrepancy are possible. One possible explanation is that the scanning curve with a returning point at 0.50 actually involves cavitation, but that the volume of capillary water that cavitates is too small for us to observe it. That may be due to the fact that, given the high specific surface areas of cement paste, at 50% RH, water is mostly adsorbed on surfaces and the amount of capillary water is too small with respect to the experimental resolution. A second possible explanation is related to the kinetics of moisture transport during the sorption measurement. Indeed, as narrow spaces, and especially the C–S–H interlayer space, exhibit slow moisture transport, only a little amount of water may have penetrated the C–S–H gel pores through interlayer spaces during the sorption measurement with a returning point at 0.50 RH, which explains why we observe a "delayed" water migration into gel pores during sorption measurement. It should be noted that, based on ^{1}H-NMR relaxometry monitoring during the saturation process of oven-dried hcp samples [19], water was observed to penetrate firstly into coarser pores (whose diameter is greater than 10 nm) and then to get absorbed from the coarser pores into finer ones (whose diameter is smaller than 10 nm). Equilibrium took about 12 days. Therefore, it is possible that, even if the water vapor started diffusing into gel pores, due to such lower rates of transport the cavitation could not be observed in the sorption isotherm with a returning point at 0.65.

3.3 Length change isotherm

Figure 5 shows the results of sorption isotherm and length-change isotherm for samples W55-11 (i.e., the well-hydrated cement paste sample conditioned at 11% RH for 2 years), W55SRA-11 (i.e., the well-hydrated cement paste containing a shrinkage reducing agent and conditioned at 11% RH for 2 years), and the monolithic MCM-41 sample obtained by compaction. As shown in Fig. 5 top left and bottom left, upon desorption, the SRA can reduce both the shrinkage and the adsorbed amounts at a relative humidity of about 0.40. As the SRA molecules make the surface of the pores hydrophobic, they mitigate the occurrence of cavitation at a relative humidity of 0.40, shifting it to larger relative humidities (see Fig. 3). Based on this fact, we infer that the negative pressure acting on the liquid water remaining in the pores of sample W55-11 around a relative humidity of 0.40 is responsible for the additional shrinkage of this sample at this relative humidity, when compared to sample W55SR-11. Therefore, the shrinkage of sample W55-

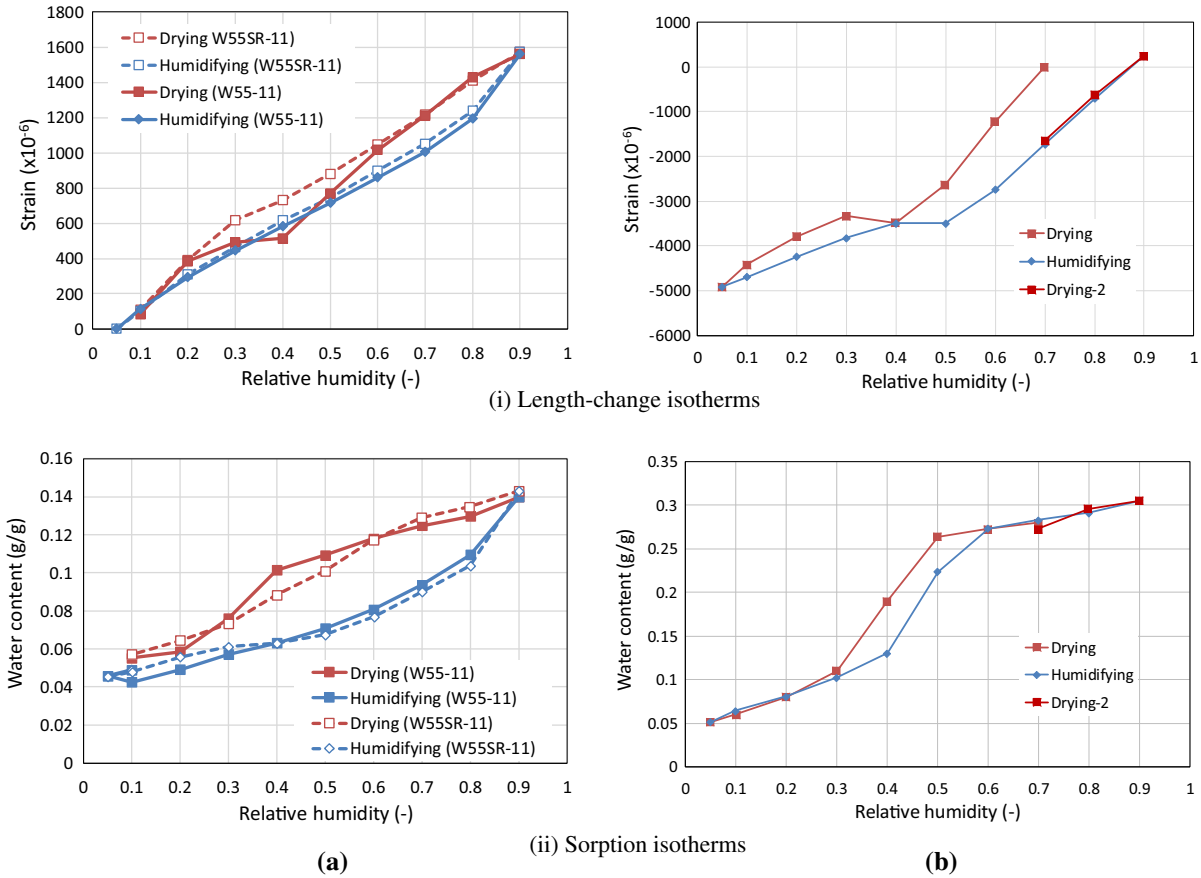

Fig. 5 Length change isotherms (**i**) and sorption isotherms (**ii**) for samples W55-11, W55-SR-11 (**a**) and for the monolithic MCM-41 sample obtained by compaction (**b**). The data for samples W55-11 and W55SR-11 are from Ref. [13]

11 upon desorption is larger than that of W55SR-11 around a relative humidity of 0.40, because the pore liquid water left in sample W55-11 was in negative pressure because of capillary tension. Such interpretation is also supported by the fact that expansion was observed in sample W55-11 in the drying step at 0.30 RH on the desorption branch, as shown in Fig. 6a, which can be explained by the vanishing of pore water due to cavitation. Such behavior contrasts with the behavior observed for sample W55SRA-11, for which no such expansion was confirmed, as shown in Fig. 6b.

For the sake of comparison, a complementary experiment was conducted with the monolithic MCM-41 sample obtained by compaction. The results are shown in Fig. 5 top and bottom right and in Fig. 6c. As MCM-41 is a regular meso-porous material (i.e., with no necks), it exhibits no cavitation [10]. The hysteretic behavior of the sorption isotherm of the monolithic MCM-41 sample was confirmed in the range of relative humidities between 0.3 and 0.6, as shown in Fig. 5 bottom right. The corresponding length change isotherm is displayed in Fig. 5 top right, which shows a slight expansion after vanishing of pore capillary water. Such behavior is well-known for porous glasses [46] and for granular zinc-chloride activated carbons [47], for which the negative pressure in the condensed liquid capillary water produces the additional length change, that comes in addition to the length change due to surface energy variations caused by water vapor sorption on pore surfaces. It should be noted that, in the case of the monolithic MCM-41 sample obtained by compaction, an expansion upon drying at 30% RH as well as a shrinkage upon humidification at 0.50 RH were observed. Such observations provide evidence that capillary condensation is always associated with a variation of the length of the sample, if the corresponding pores are reasonably small and if the induced negative pressures in the liquid are large enough for

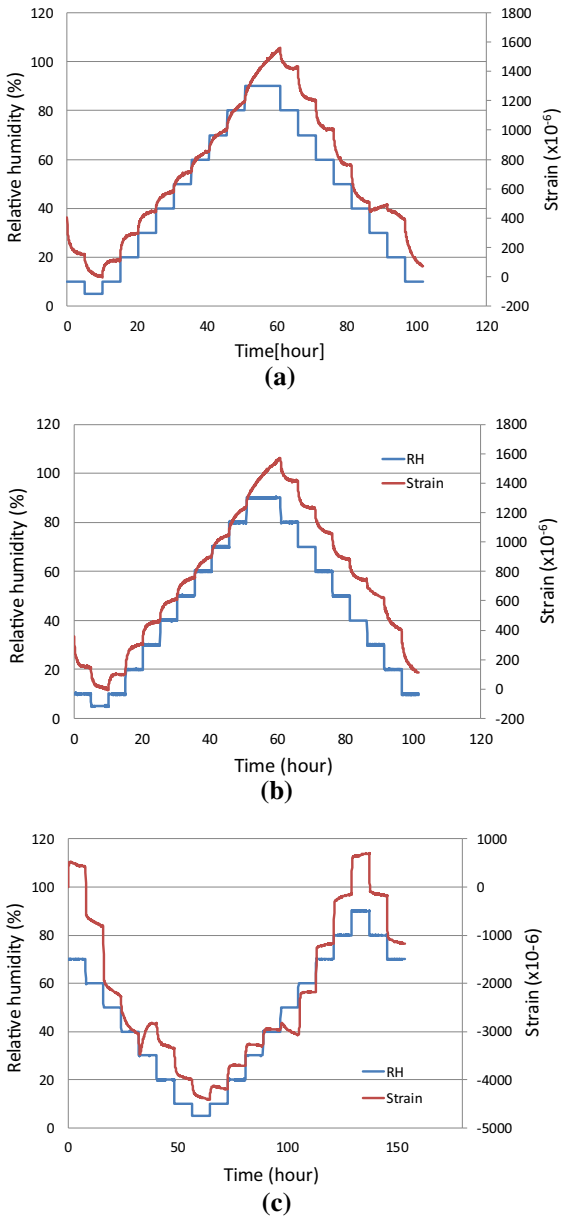

Fig. 6 Length change as a function of experimental elapsed time **a** W55-11, **b** W55SR-11, **c** monolithic MCM-41 samples obtained by compaction

the corresponding deformations to be observable. In contrast, no shrinkage was observed for sample W55-11, which suggests that the kinetics of moisture transport in the mid-range of relative humidities during the humidifying process was slow enough not to induce such shrinkage. Such interpretation is consistent with the one given to explain the discrepancy between the minimum size of the pores in which cavitation should be observed and the minimum size of the pores in which we indeed observed cavitation (see Fig. 4).

4 Conclusion

We discussed the cavitation phenomenon in hardened cement paste during short-term water vapor desorption measurement, by using experimental data of sorption isotherms at various temperatures, scanning isotherms, and length-change isotherms. Hierarchical zeolites, portlandite, and MCM-41 were used for comparison. Based on the experimental data and the related discussions, a sudden drop of the adsorbed amount at a relative humidity of 0.35 in the desorption branch at 20 °C was identified as caused by cavitation. Cavitation in hardened cement paste occurs in pores constricted by smaller pores whose size should be less than 2.05 nm, these latter being identified as C–S–H interlayer space. The pores in which cavitation occurs are likely to be C–S–H gel pores. We observed no cavitation in pores whose diameter was smaller than $5 \sim 6$ nm, while theory and experimental results obtained on other materials show that the diameter of the smallest pores in which cavitation occurs should be significantly smaller.

Acknowledgements A part of this research is supported by JSPS KAKENHI grant number 18H03804. The used materials and facilities are supported by the Nuclear Regulatory Authority (NRA, Japan) and JSPS KAKENHI grant number 15H04077.

Compliance with ethical standards

Conflict of interest The authors have no conflict of interest directly relevant to the content of this article.

References

1. Jesser L (1927) Kolloide Chemische Reaktionen des Tonerdezementmörtels. Zement 16:741
2. Feldman RF, Sereda PJ (1964) Sorption of water on compacts of bottle-hydrated cement. I. The sorption and length-

change isotherms. J Appl Chem 14(2):87–93. https://doi.org/10.1002/jctb.5010140206
3. Baroghel-Bouny V (2007) Water vapour sorption experiments on hardened cementitious materials: Part I: Essential tool for analysis of hygral behaviour and its relation to pore structure. Cem Concr Res 37(3):414–437. https://doi.org/10.1016/j.cemconres.2006.11.019
4. Brunauer S, Mikhail RS, Bodor EE (1967) Some remarks about capillary condensation and pore structure analysis. J Colloid Interface Sci 25(3):353–358. https://doi.org/10.1016/0021-9797(67)90041-0
5. Libby B, Monson PA (2004) Adsorption/desorption hysteresis in inkbottle pores: a density functional theory and Monte Carlo simulation study. Langmuir 20(10):4289–4294. https://doi.org/10.1021/la036100a
6. Thommes M, Smarsly B, Groenewolt M, Ravikovitch PI, Neimark AV (2006) Adsorption hysteresis of nitrogen and argon in pore networks and characterization of novel micro- and mesoporous silicas. Langmuir 22(2):756–764. https://doi.org/10.1021/la051686h
7. Morishige K, Fujii H, Uga M, Kinukawa D (1997) Capillary critical point of argon, nitrogen, oxygen, ethylene, and carbon dioxide in MCM-41. Langmuir 13(13):3494–3498. https://doi.org/10.1021/la970079u
8. Coasne B, Galarneau A, Pellenq RJ, Di Renzo F (2013) Adsorption, intrusion and freezing in porous silica: the view from the nanoscale. Chem Soc Rev 42:4141–4171. https://doi.org/10.1039/c2cs35384a
9. Coasne B (2016) Multiscale adsorption and transport in hierarchical porous materials. New J Chem 40(5):4078–4094. https://doi.org/10.1039/C5NJ03194J
10. Lépinay M, Broussous L, Licitra C, Bertin F, Rouessac V, Ayral A, Coasne B (2015) Predicting adsorption on bare and modified silica surfaces. J Phys Chem C 119(11):6009–6017. https://doi.org/10.1021/jp511726a
11. Maruyama I, Nishioka Y, Igarashi G, Matsui K (2014) Microstructural and bulk property changes in hardened cement paste during the first drying process. Cem Concr Res 58:20–34. https://doi.org/10.1016/j.cemconres.2014.01.007
12. Maruyama I, Sakamoto N, Matsui K, Igarashi G (2016) Microstructural changes in white Portland cement paste under the first drying process evaluated by WAXS, SAXS, and USAXS. Cem Concr Res 91:24–32. https://doi.org/10.1016/j.cemconres.2016.10.002
13. Maruyama I, Beppu K, Kurihara R, Furuta A (2016) Action mechanisms of shrinkage reducing admixture in hardened cement paste. J Adv Concr Technology 14(6):311–323. https://doi.org/10.3151/act.14.311
14. Feldman RF, Sereda PJ (1968) A model for hydrated Portland cement paste as deduced from sorption-length change and mechanical properties. Mat Constr 1(6):509–520. https://doi.org/10.1007/BF02473639
15. Zhang J, Scherer GW (2011) Comparison of methods for arresting hydration of cement. Cem Concr Res 41(10):1024–1036. https://doi.org/10.1016/j.cemconres.2011.06.003
16. Gallucci E, Zhang X, Scrivener KL (2013) Effect of temperature on the microstructure of calcium silicate hydrate (C–S–H). Cem Concr Res 53:185–195. https://doi.org/10.1016/j.cemconres.2013.06.008
17. Bahafid S, Ghabezloo S, Duc M, Faure P, Sulem J (2017) Effect of the hydration temperature on the microstructure of Class G cement: C–S–H composition and density. Cem Concr Res 95:270–281. https://doi.org/10.1016/j.cemconres.2017.02.008
18. Bahafid S, Ghabezloo S, Faure P, Duc M, Sulem J (2018) Effect of the hydration temperature on the pore structure of cement paste: experimental investigation and micromechanical modelling. Cem Concr Res 111:1–14. https://doi.org/10.1016/j.cemconres.2018.06.014
19. Gajewicz AM, Gartner E, Kang K, McDonald PJ, Yermakou V (2016) A 1H NMR relaxometry investigation of gel-pore drying shrinkage in cement pastes. Cem Concr Res 86:12–19. https://doi.org/10.1016/j.cemconres.2016.04.013
20. Wyrzykowski M, McDonald PJ, Scrivener KL, Lura P (2017) Water redistribution within the microstructure of cementitious materials due to temperature changes studied with 1H NMR. J Phys Chem C 121(50):27950–27962. https://doi.org/10.1021/acs.jpcc.7b08141
21. Thommes M, Mitchell S, Pérez-Ramírez J (2012) Surface and pore structure assessment of hierarchical MFI zeolites by advanced water and argon sorption studies. J Phys Chem C 116(35):18816–18823. https://doi.org/10.1021/jp3051214
22. Aili A, Vandamme M, Torrenti J-M, Masson B (2018) Is long-term autogenous shrinkage a creep phenomenon induced by capillary effects due to self-desiccation? Cem Concr Res 108:186–200. https://doi.org/10.1016/j.cemconres.2018.02.023
23. Speedy RJ (1982) Limiting forms of the thermodynamic divergences at the conjectured stability limits in superheated and supercooled water. J Phys Chem 86(15):3002–3005. https://doi.org/10.1021/j100212a038
24. Yamada M, Mossa S, Stanley HE, Sciortino F (2002) Interplay between time–temperature transformation and the liquid–liquid phase transition in water. Phys Rev Lett 88(19):195701. https://doi.org/10.1103/PhysRevLett.88.195701
25. Herbert E, Balibar S, Caupin F (2006) Cavitation pressure in water. Phys Rev E 74(4):041603
26. Caupin F (2005) Liquid-vapor interface, cavitation, and the phase diagram of water. Phys Rev E 71(5):051605. https://doi.org/10.1103/PhysRevE.71.051605
27. Caupin F, Herbert E (2006) Cavitation in water: a review. C R Phys 7(9):1000–1017. https://doi.org/10.1016/j.crhy.2006.10.015
28. Badmann R, Stockhausen N, Setzer MJ (1981) The statistical thickness and the chemical potential of adsorbed water films. J Colloid Interface Sci 82(2):534–542. https://doi.org/10.1016/0021-9797(81)90395-7
29. Daimon M, Abo-El-Enein SA, Rosara G, Goto S, Kondo R (1977) Pore structure of calcium silicate hydrate in hydrated tricalcium silicate. J Am Ceram Soc 60(3–4):110–114. https://doi.org/10.1111/j.1151-2916.1977.tb15483.x
30. Powers TC, Brownyard TL (1946) Studies of the physical properties of hardened portland cement paste part 1. A review of methods that have been used for studying the physical properties of hardened cement paste. J Am Concr Inst 18(2):101–132
31. Feldman RF (1980) Application of the helium inflow technique for measuring surface area and hydraulic radius of

hydrated portland cement. Cem Concr Res 10(5):657–664. https://doi.org/10.1016/0008-8846(80)90029-0
32. Brunauer S, Mikhail RS, Bodor EE (1967) Pore structure analysis without a pore shape model. J Colloid Interface Sci 24(4):451–463. https://doi.org/10.1016/0021-9797(67)90243-3
33. Barbič L, Kocuvan I, Blinc R, Lahajnar G, Merljak P, Zupancic I (1982) The determination of surface development in cement pastes by nuclear magnetic resonance. J Am Ceram Soc 65(1):25–31. https://doi.org/10.1111/j.1151-2916.1982.tb09917.x
34. Blinc R, Lahajnar G, Žumer S, Pintar MM (1988) NMR study of the time evolution of the fractal geometry of cement gels. Phys Rev B 38(4):2873–2875. https://doi.org/10.1103/PhysRevB.38.2873
35. Korb JP (2009) NMR and nuclear spin relaxation of cement and concrete materials. Curr Opin Colloid Interface Sci 14(3):192–202. https://doi.org/10.1016/j.cocis.2008.10.004
36. McDonald PJ, Rodin V, Valori A (2010) Characterisation of intra- and inter—C–S–H gel pore water in white cement based on an analysis of NMR signal amplitudes as a function of water content. Cem Concr Res 40(12):1656–1663. https://doi.org/10.1016/j.cemconres.2010.08.003
37. Valori A, Rodin V, McDonald PJ (2010) On the interpretation of 1H 2-dimensional NMR relaxation exchange spectra in cements: is there exchange between pores with two characteristic sizes or Fe^{3+} concentrations? Cem Concr Res 40(9):1375–1377. https://doi.org/10.1016/j.cemconres.2010.03.022
38. Muller ACA, Scrivener KL, Gajewicz AM, McDonald PJ (2013) Densification of C–S–H Measured by 1H NMR relaxometry. J Phys Chem C 117(1):403–412. https://doi.org/10.1021/jp3102964
39. Muller ACA, Scrivener KL, Gajewicz AM, McDonald PJ (2013) Use of bench-top NMR to measure the density, composition and desorption isotherm of C-S–H in cement paste. Microporous Mesoporous Mater 178:99–103. https://doi.org/10.1016/j.micromeso.2013.01.032
40. Valori A, McDonald PJ, Scrivener KL (2013) The morphology of C–S–H: lessons from 1H nuclear magnetic resonance relaxometry. Cem Concr Res 49:65–81. https://doi.org/10.1016/j.cemconres.2013.03.011
41. McDonald PJ, Korb JP, Mitchell J, Monteilhet L (2005) Surface relaxation and chemical exchange in hydrating cement pastes: a two-dimensional NMR relaxation study. Phys Rev E 72(1):011409. https://doi.org/10.1103/PhysRevE.72.011409
42. Haynes WM (2014) CRC handbook of chemistry and physics. CRC Press, Boca Raton
43. Powers TC, Brownyard TL (1946–1947) Studies of the physical properties of hardened portland cement paste, Part 1–9. J Am Concr Inst 43:101–133, 249–337, 469–504, 549–602, 669–712, 845–857, 933–969, 972–990
44. Bunkin NF, Kiseleva OA, Lobeyev AV, Movchan TG, Ninham BW, Vinogradova OI (1997) Effect of salts and dissolved gas on optical cavitation near hydrophobic and hydrophilic surfaces. Langmuir 13(11):3024–3028. https://doi.org/10.1021/la960265k
45. Morishige K, Ito M (2002) Capillary condensation of nitrogen in MCM-41 and SBA-15. J Chem Phys 117(17):8036–8041. https://doi.org/10.1063/1.1510440
46. Amberg CH, McIntosh R (1952) A study of adsorption hysteresis by means of length changes of a rod of porous glass. Can J Chem 30(12):1012–1032. https://doi.org/10.1139/v52-121
47. Haines RS, Intosh R (1947) Length changes of activated carbon rods caused by adsorption of vapors. J Chem Phys 15(1):28–38. https://doi.org/10.1063/1.1746282
48. Maruyama I, Gartner E, Beppu K, Kurihara R (2018) Role of alcohol-ethylene oxide polymers on the reduction of shrinkage of cement paste. Cem Concr Res 111:157–168. https://doi.org/10.1016/j.cemconres.2018.05.017